Experimental Comparison of Vasculature Segmentation Methods

Yuchun Ding and Li Bai
School of Computer Science, Nottingham University, Wollaton Road, Nottingham, U.K.

Keywords: Vascular Segmentation, Retinal Vasculature, Micro-CT.

Abstract: Vessel segmentation algorithms play a very important role in vascular disease diagnosis and prediction. Current vessel segmentation research uses mostly images of large vessels, which are relatively easy to extract, but segmenting microvasculature is more challenging and very important for analysing vascular disease such as Alzheimer's Diseases. The aim of this paper is to report experimental results of several common vessel image segmentation methods. Retinal vessel image database DRIVE is used for 2D experiments and a micro-CT image is used for 3D experiments.

1 INTRODUCTION

Vascular pathology is present in most human diseases, so there has been intense research in the past in Magnetic Resonance Imaging (MRI) for diagnosis and treatment of vascular diseases. Recently the role of neurovascular dysfunction has been identified, including Alzheimer's Diseases (AD). A significant finding is that vascular abnormalities and angiogenesis could potentially serve as an early biomarker of the diseases. But the lack of computational tools is becoming increasingly apparent. A feasible way to validate the theory linking microvasculature to pathology of neurodegenerative conditions on large datasets is to develop an automated computational analysis method. However, existing algorithms for image analysis have mostly been developed for segmenting large vessels, and analysis of these vessels has been limited to measuring curvature and diameter of individual vessels, which are unsuitable for microvasculature. Imaging devices such as micro-CT can achieve resolutions on the order of several μm, allowing imaging the three dimensional (3D) microvasculature down to the capillary level. The main weakness of using micro-CT for vascular research is considered to be the lack of software for 3D quantification of microvasculature. Four well-known segmentation methods were investigated, which include local entropy thresholding (LET), level set methods, vesselness filter, and wavelet transform modulus maxima (WTMM). All of these are well-performed on 2D retinal images and the aim of this paper is to review, analyse and compare the vessel segmentation methods in both 2D and 3D vessel images and to show the microvasculature detection performance of each method.

2 METHODS

2.1 Image Databases

We have chosen the retinal vessel image from a publicly available database DRIVE (Staal et al., 2004) for our 2D experiments because it is a commonly used database for previous research on vessel segmentation. The database is made up of 40 images that have been randomly selected from a diabetic retinopathy (DR)-screening program. Each image has a dimension of 565 by 584 pixels. For each image in the test set, two manual segmentations of blood vessels are available. The second set of manual segmented image will be used in this investigation because is it the observer results most commonly used when comparing effectiveness of method.

As the existing publicly available brain vasculature dataset such as MRI, CTA or MRA images only contain large vessels, which is not possible for analysing the microvasculature, a corrosion casting method was used to prepare 3-D resin casts of the microvasculature of wild type and transgenic Alzheimer mice model brains (Bedford et al., 2008). The animals were lightly fixed in 4% paraformaldehyde by transcardiac perfusion at

Ding Y. and Bai L..
Experimental Comparison of Vasculature Segmentation Methods.
DOI: 10.5220/0004648804250432
In *Proceedings of the 9th International Conference on Computer Vision Theory and Applications* (VISAPP-2014), pages 425-432
ISBN: 978-989-758-003-1

120mmHg prior to delivery of fluorescent PN4 resin via a syringe pump. After 48hr curing time, the brains were removed and macerated in 10% KOH for a period of 2 weeks at 37°C. The resin casts were thoroughly washed in DDH2O and immersed in 2% Os04 for a further 3 days then washed and freeze dried for micro-CT (Skyscan 1174) scanning. Measurements were obtained at a voltage of 40 kV, current of 800 μA and voxel resolution of 24 μm.

Figure 1 shows a 3D view of the original Micro-CT scanned image of dimension $305 \times 305 \times 320$ pixels visualised using MRIcron (Rorden et al., 2007). Due to limitations of the viewer selected, those faint and narrow vessels with low contrast are barely visible, a simple thresholding method was applied to reveal the vessels in the image for the purpose of visualisation. The image on the right in Figure 1 shows the expected resulting image.

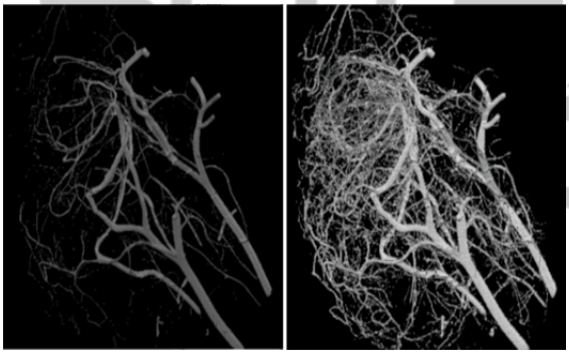

Figure 1: Original Image (left), Enhanced Image (right).

2.2 Image Enhancement

A review of retinal blood vessel segmentation using images from the DRIVE database has shown that most of the vessel image segmentation algorithms could only achieve 70% and 80% of blood-vessel pixel are correctly classified (Fraz et al., 2012). This is due to the difficulty of visualising small vessels in images. As such, it is desirable to enhance the vessels in images prior to segmentation. The paper uses following enhancement methods.

2.2.1 Gabor Filter

The Gabor filter is a Gaussian kernel function modulated by a sinusoidal plane wave in 2D and it is capable of tuning a signal to specific frequencies (Daugman, 1988). The Gabor filter that we use for our work (blood vessel enhancement) can be represented by:

$$g_{\{\lambda,\theta,\varphi,\sigma,\gamma\}}(x,y) = \exp\left(-\frac{x'^2+\gamma^2 y'^2}{2\sigma^2}\right)\cos\left(2\pi\frac{x'}{\lambda}+\varphi\right) \quad (1)$$

$$x' = x\cos\theta + y\sin\theta \quad (2)$$

$$y' = -x\sin\theta + y\cos\theta \quad (3)$$

where λ is the wavelength of the cosine factor, θ specifies the filter direction, φ is a constant representing the phase offset, γ represents spatial aspect ratio, with σ as the standard deviation of the filter's Gaussian factor.

2.2.2 Matched Filter

Matched filter convolves a signal with a designed kernel and extracts information (from that signal) which matches the kernel. Based on the fact that those blood vessels are typically line-like, with small curvatures and usually have a relatively low contrast, a matched filter kernel was given that matched the multiple intensity profile of the vessels' cross section rather than a single one (Pająk, 2003):

$$f(x,y) = -exp\left(\frac{-x^2}{2\sigma^2}\right), for\ |y| \le L/2, \quad (4)$$

Here, σ defines the spread of the intensity profile and L is the length of the segment. It is assumed that a fixed vessel has orientation along the y-axis. In reality, vessels are oriented in many different directions, so a set of kernels is applied at each pixel and only the maximum response is retained.

2.3 Segmentation

This section reviews four vessel segmentation methods, and describes our own experiments with the methods.

2.3.1 Local Entropy Thresholding

2.3.1.1 Theory

Local entropy thresholding (LET) was proposed for segmenting retinal blood vessels (Chanwimaluang and Fan, 2003). The key point of this method is to automatically estimate the threshold value, based on the entropy of an image, using a co-occurrence matrix. A gray level co-occurrence asymmetric matrix t_{ij} is created to indicate spatial structural information of an image – the $(i,j)th$ entry of the matrix that gives the number of times the gray level j follows the gray level i:

$$t_{ij} = \sum_{l=1}^{P}\sum_{k=1}^{Q}\delta \quad (5)$$

where

$$\delta = 1\ if \begin{cases} f(l,k) = i\ and\ f(l,k+1) = j \\ or \\ f(l,k) = i\ and\ f(l+1,k) = j \end{cases}$$
$$\delta = 0\ otherwise$$

Let s be the threshold such that $0 \le s \le L-1$. Then threshold s partitions the co-occurrence matrix (Pal and Pal. 1989), into 4 quadrants, namely A, B, C, and D, as shown in Figure 2, where A and C represent gray level transition within the vessel object and background respectively. The gray level transition between the vessel object and background are placed in quadrant B and D.

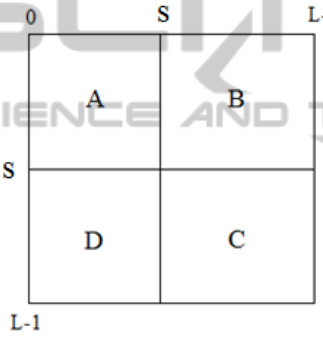

Figure 2: Quadrants of co-occurrence matrix.

The normalised probabilities of each quadrant are defined as:

$$P_{i,j}^{A} = \frac{P_{i,j}}{P_A} = \frac{t_{ij}}{\sum_{i=0}^{s}\sum_{j=0}^{s} t_{ij}} \quad (6)$$
$$for\ 0 \le i \le s, 0 \le j \le s$$

$$P_{i,j}^{C} = \frac{P_{i,j}}{P_C} = \frac{t_{ij}}{\sum_{i=s+1}^{L-1}\sum_{j=s+1}^{L-1} t_{ij}} \quad (7)$$
$$for\ s+1 \le i \le L-1, s+1 \le j \le L-1$$

Where p_{ij} is the probability of co-occurrence of gray levels i and j. P_A and P_C are the probabilities of vessel object and background.
Hence, the total second-order local entropy of the object and background can be written as:

$$H_T^{(2)}(s) = H_A^{(2)}(s) + H_C^{(2)}(s) \quad (8)$$

$$H_A^{(2)}(s) = -\frac{1}{2}\sum_{i=0}^{s}\sum_{j=0}^{s} P_{ij}^{A}\log_2 P_{ij}^{A} \quad (9)$$

$$H_C^{(2)}(s) = -\frac{1}{2}\sum_{i=s+1}^{L-1}\sum_{j=s+1}^{L-1} P_{ij}^{C}\log_2 P_{ij}^{C} \quad (10)$$

The gray level corresponding to the maximum of $H_T^{(2)}(s)$ gives the optimal threshold for vessel and non-vessels classification. Then length filtering is used to remove misclassified pixel.

2.3.1.2 Experiment

For testing the performance of LET, we choose matched filter followed by Gabor filter for vessel enhancement (Ding et al., 2013). Gabor filters parameters are selected using a genetic algorithm tool in MATLAB. The algorithm continually reproduces a new generation of 'offsprings', which inherit features from the previous generation and eventually leads to an optimal solution.

The proposed method retains the computational simplicity and straightforwardness and at the same time achieves accurate segmentation results of retinal images. Using a genetic algorithm can help to find good parameters for the filter but it is also time consuming, technically the selected value can be only used for specific image of current interest.

Figure 4 clearly shows that LET with the Gabor filter performed very well compared to LET, as shown in Figure 3. More narrow vessels are detected although few non-vessel pixels are incorrectly classified. 3D enhancement was not implemented as it is not sufficient to convolve all 26 directions. Figure 5 visualised the result of LET without pre-processing the image and many narrow vessels were misclassified. The drawback of the LET method is that it is not scale-invariant and does not handle vessels of different parameters well.

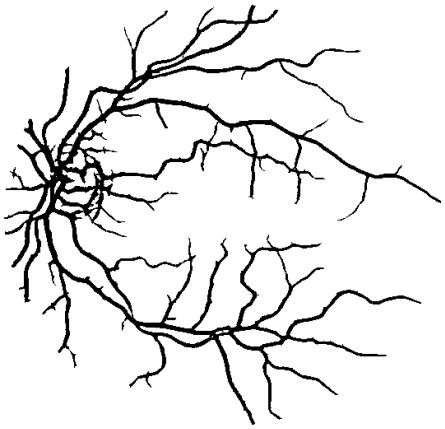

Figure 3: Result of LET without Gabor Filter in 2D.

Figure 4: Result of LET with Gabor Filter in 2D.

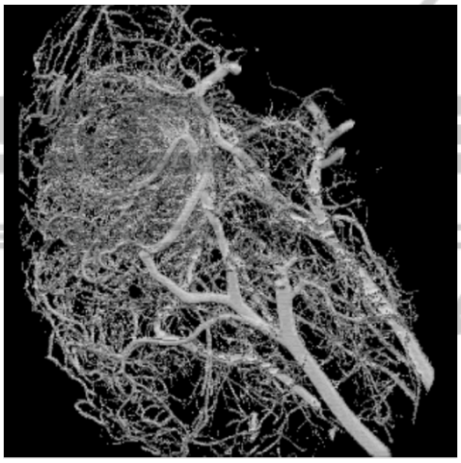

Figure 5: Result of LET in 3D.

2.3.2 Level Set

2.3.2.1 Theory

The level set method is a powerful mathematical and computational tool for tracking the evolution of curves/surfaces. The basic idea of the method is to evolve a curve by applying forces normal to the surface and the contour evolution stops at positions where the values of gradient magnitude are large. This method is fast on regular image but it often fails at low contrast edges or gaps in the object as it is highly dependent on image contrast; as a result, the evolving contour simply leaks through the gaps and the object is represented by incomplete contours in some particular fashion.

A complex level set method was introduced based on local phase (Lathen et al., 2008). Because vessels appear either as lines or edge pairs with varying widths and contrasts, the method uses the outcome of quadrature filters as a complex valued filter pair consisting of a line filter as real part and an edge filter as imaginary part. The filtered signal is strongly "line-like" when the filter response is purely real, is edge-like when it is purely imaginary. The magnitude of the filter response gives the strength of the structure, while the angle (local phase, the argument of the complex value) of the response indicates whether it is line or edge. Because it is independent of signal strength, the local phase as a line/edge detector is invariant to image contrast, making it more powerful when compared to gradient-based edge detectors. Multiscale is then achieved using a weighted sum over all scales, and normalisation is applied to the output. The outcome is a "global" phase that can be used to drive a contour robustly towards the vessel edges.

Then a level set method (Osher and Sethian, 1988) for front propagation is used to relate to the phase based edge detector (global phase map). The idea is to use the real part of the phase map as a speed function. This is expressed by:

$$\frac{\partial \phi}{\partial t} = -Re\left(\hat{q}(\sigma)\right)|\nabla\phi| + \alpha\kappa|\nabla\phi| \qquad (11)$$

Where $\hat{q}$ denotes the normalized phase map, α is a regularisation parameter and κ is curvature.

2.3.2.2 Experiment

The local phase method described can distinguish line and edge by taking local phase into account. Most importantly, it halts the evolving contour at the end of the vessel to prevent leakage. Although the method succeeds in object and motion segmentation, it fails for images that contain faint and narrow vessel pixels, leading to the level set terminating early and leaving many vessels undetected, as shown in Figure 6.

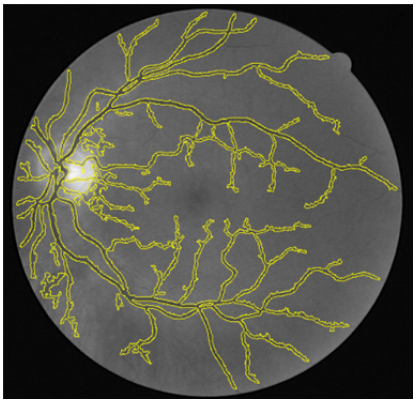

Figure 6: Result of Phased Based Level Set.

In our experiment we use matched filter to enhance vessel image before level set segmentation. Figure 7

shows the result image using level set with matched filtered image, many faint vessels were detected, although level set contour was not terminated at few background pixels.

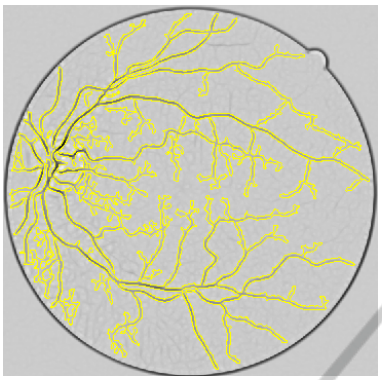

Figure 7: Result of our method.

We have failed to complete the experiment using 3D images because of high computational cost. The image shown in Figure 8 is the 3D segmentation result after 30 minutes implementation.

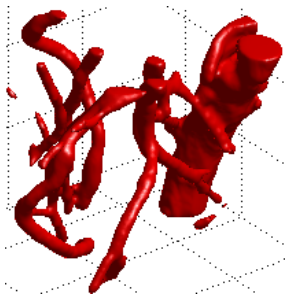

Figure 8: Result of Level Set in 3D.

2.3.3 Multiscale Vesselness Filter

2.3.3.1 Theory

The multiscale second order local structure of an image (Hessian) is examined to develop a vessel enhancement filter (Frangi et al., 1998). A vesselness measure is obtained from all eigenvalues of the Hessian to determine a pixel is plate-like (Sato et al., 1998), tubular-like or blob-like. Let λ_k be the eigenvalue with the k-th smallest magnitude, for an ideal tubular structure in a 3D image, given as:

$$\begin{matrix} |\lambda_1| \leq |\lambda_2| \leq |\lambda_3| \\ |\lambda_1| \approx 0, |\lambda_1| \ll |\lambda_2|, \lambda_2 \approx \lambda_3 \end{matrix} \quad (12)$$

The vesselness function is then defined by probability-like estimates of vesselness according to two geometric ratios (R_A *and* R_B) to ensure that only the geometric information of the image is captured:

$$V_0(s) = \begin{cases} 0 & if\ \lambda_2 > 0\ or\ \lambda_3 > 0, \\ \left(1 - \exp\left(-\frac{{R_A}^2}{2\alpha^2}\right)\right) \exp\left(-\frac{{R_B}^2}{2\beta^2}\right) \left(1 - \exp\left(-\frac{S^2}{2c^2}\right)\right) & \end{cases} \quad (13)$$

where $R_A = \frac{|\lambda_2|}{|\lambda_3|}, R_B = \frac{|\lambda_1|}{\sqrt{|\lambda_2 \lambda_3|}}, S = \sqrt{\sum_{j \leq D} \lambda_j^2}$

R_A refers to the largest area cross section of the ellipsoid, used for distinguishing between plate-like and line like structure, while R_B accounts for the deviation from a blob-like structure but cannot distinguish between a line and a plate like pattern, S is defined using Frobenius matrix norm to control the sensitivity of $V_0(s)$ to background noise. Here D is the dimension of the image. This measurement will give a high value for regions with high contrast and a low value for the background where no structure is present. a, b and c are thresholds which control the sensitivity of the line filter to the measures R_A, R_B and S. The equation for 2D images follows from the same reasoning as in 3D where $R_B = \frac{\lambda_1}{\lambda_2}$.

$$V_0(s) = \begin{cases} 0 & if\ \lambda_2 > 0\ , \\ \exp\left(-\frac{{R_B}^2}{2\beta^2}\right)\left(1 - \exp\left(-\frac{S^2}{2c^2}\right)\right) & \end{cases} \quad (14)$$

A final estimate of vesselness will then be integrated with the filter responses at different scales s as vessels appearing in varying width.

2.3.3.2 Experiment

The advantages of the vesselness filter are that it is fast, simple, and accurate, as shown in Figure 9.

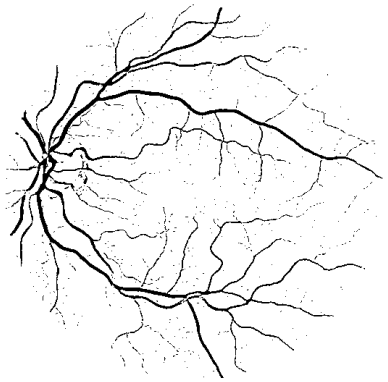

Figure 9: Result of Vesselness Filter in 2D.

It can also be utilised for separating arteries or muscles from veins using specified scale values. Figure 10 shows the 3D result that uses two different scale values. 3D vesselness filter is a most commonly used methods for enhancing or extracting vasculature, although it still suffers from two major drawbacks. It is not scale invariant: user interaction is required for selecting the range of scales, although it is very difficult to adjust the value; It does not perform well on retinal images with massive amount of lesions, therefore pre-processing is required.

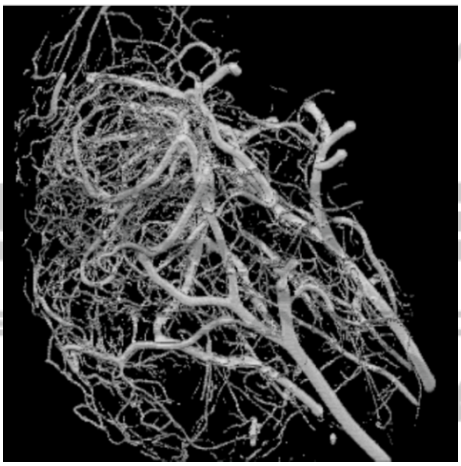

Figure 10: Result of Vesselness Filter in 3D.

2.3.4 WTMM

2.3.4.1 Theory

A multiscale edge detection algorithm was developed base on wavelet transform modulus maxima (Mallat and Sifen, 1992). The method can detect the irregularities (edges) in an image with slight noise and without intensity inhomogeneity. Suppose $\phi(x,y)$ is a smooth two-dimensional differentiable function, then a two dimensional wavelet (e.g. Gaussian) can be defined as $\phi^x(x,y)$ and $\phi^y(x,y)$ where:

$$\phi^x(x,y) = \frac{\partial\phi(x,y)}{\partial x},\ \phi^y(x,y) = \frac{\partial\phi(x,y)}{\partial y} \quad (15)$$

The wavelet transformation uses only two components $\left|{W_{2^j}}^x f(x,y)\right|^2$ and $\left|{W_{2^j}}^y f(x,y)\right|^2$, in dyadic scales:

$$\begin{vmatrix} W_{2^j}^x f(x,y) \\ W_{2^j}^y f(x,y) \end{vmatrix} = 2^j \begin{vmatrix} \frac{\partial\left(f * \phi_{2^j}\right)(x,y)}{\partial x} \\ \frac{\partial\left(f * \phi_{2^j}\right)(x,y)}{\partial y} \end{vmatrix} \quad (16)$$

Here * expresses the convolution. Wavelet transform modulus and gradient direction at each scale 2^j are defined by:

$$M_{2^j} f(x,y) = \sqrt{|{W_{2^j}}^x f(x,y)|^2 + |{W_{2^j}}^y f(x,y)|^2} \quad (17)$$

$$A_{2^j}{}^x f(x,y) = \arctan\left(\frac{{W_{2^j}}^x f(x,y)}{{W_{2^j}}^y f(x,y)}\right) \quad (18)$$

For any point in the original image, two neighbourhoods along the gradient direction are compared. If edge intensity $M_{2^j} f(x,y)$ is local maxima, it is retained and considered as an edge pixel, otherwise the point will be deleted. Following this, a threshold value is chosen to filter out the noise.

2.3.4.2 Experiment

Figure 11 shows that method is much likely to be a Canny edge detector. Figure 12 shows the output using WTMM on 3D image. The image size is much increased in the transition of the problem from 2D to 3D, and so more problems with the methods occur. For instance, the computational time was exponentially increased with the size of image. When the scales were large, thin vessels were blurred due to the large Gaussian window convolution, which unable to show the analytical model due to the removal of crispness of the thin vessels. Thus these thin vessels appear to be a slightly broader, when compared to the results of thresholding schemes.

The major advantage of the system was its simplicity in implementation. The drawback of this method is that edges found are not connected, and also it is susceptible to errors for noisy images.

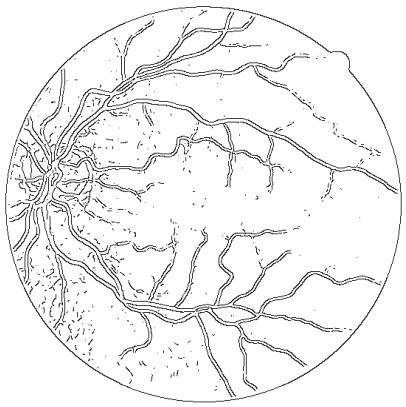

Figure 11: Result of WTMM in 2D.

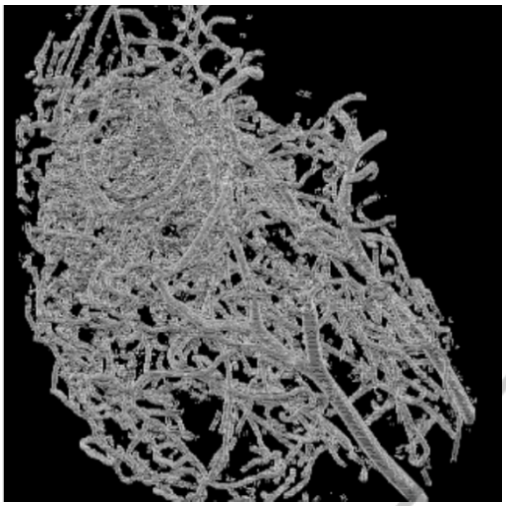

Figure 12: Result of WTMM in 3D.

3 COMPARISON AND ANALYSIS

Table 1 and 2 contain performance detail on each database separately. Performance measures are sensitivity, the percentage of correctly classified blood-vessel pixels, obtained by TP/(TP+FN); specificity, the percentage of correctly classified non-blood-vessel pixels, obtained by TN/(FP+TN); accuracy, how close the number of correctly classified pixels is to the actual value, obtained by (TP+TN)/(TP+FP+FN+TN) and precision, how close the true positive and false positive are, obtained by TP/(TP+FP); where T=TURE, F=FALSE, P=POSITIVE and N=NEGATIVE.

3.1 2D

WTMM was the fastest. The speed of the vesselness filter and LET were acceptable, but LET with Gabor filter and all level set methods are slower due to parameter selection for the Gabor filter. LET with Gabor filter achieved the highest sensitivity (89.83%). Both this method and our level set method provided higher sensitivity as more vessels are detected. WTMM and LET produced low sensitivity due to unconnected and missing vessels. Vesselness filter has produced low sensitivity (62.64%) as user selected scales and threshold values were susceptible to errors. The best specificity obtained is by the vesselness filter (98.74%), because it is robust to image noise. While improved LET, level set methods, and WTMM are sensitive to image noise. Vesselness filter produced the highest accuracy (94.25%) whilst the results of LET and WTMM are not good as a large number of vessels are missing or disconnected. Vesselness filter achieved the highest precision (87.64%).

3.2 3D

Implementation cost using vesselness filter and LET remained acceptable. WTMM took longer than 2 minutes. Both level set methods failed the segmentation because it was computationally expensive in 3D. Vesselness filter achieved the highest sensitivity (86.26%) as more small vessels were corrected detected than using LET. WTMM failed the experiment because all vessels were broader than the original vessels. All Specificity

Table 1: Performance Detail using 2D Retinal Vessel Image.

2D	Sensitivity	Specificity	Accuracy	Precision	Run time	Drawback
WTMM	0.4545	0.9518	0.8916	0.5648	0.27s	Unconnected vessels
LET	0.7599	0.9621	0.9383	0.7282	2.15s	Missing vessels
LET+Gabor Filter	0.8983	0.9435	0.9378	0.6955	16.15s	Parameter selection
Phase Based Level Set	0.8567	0.9399	0.9299	0.6626	40.53s	Early termination
PB Level Set+Matched Filter	0.8712	0.8610	0.8622	0.4631	25.46s	Non-smooth vessels
Vesselness Filter	0.6264	0.9874	0.9425	0.8764	1.05s	Need user interaction

Table 2: Performance Detail using 3D Rat Brain Vessel Image.

3D	Sensitivity	Specificity	Accuracy	Precision	Run time	Drawback
WTMM	0.4711	0.9895	0.9868	0.1889	255.35s	Thick vessels
LET	0.4181	0.9989	0.9959	0.6668	33.81s	Not scale-invariant
Vesselness Filter	0.8626	0.9985	0.9978	0.7468	74.67s	Need user Interaction

values were high as the amount of noise was very little. The highest value obtained was by LET (99.89%). Vesselness filtered image was much similar to the expected result and it obtained the best accuracy (99.78%) and precision (74.68%).

4 CONCLUSIONS

We have reviewed and analysed a number of vessel enhancement and segmentation algorithms using both 2D and 3D image. Vesselness filter can be used to detect vessels of varying scales. A potential application of this method is to extract the brain microvasculature and compare healthy and diseased brains. LET has produced the highest sensitivity in 2D experiment but this method is recommended only when the vessels are large and on a simple background. Although WTMM and level set method failed the performance tests, they are capable of detecting edges of large objects, such as brain tumours. The main issue in this work is that the performance test was not technically accurate due to the poorly made ground truth and insufficient test images so the 3D segmentation result has not been 100% validated. For further work we aim to produce valid ground truth images for testing segmentation algorithms. We will also continue to develop robust wavelet filters and in combination with other mathematical methods and metrics such as high-order flows (Lim et al, 2013) non-Euclidean distance functions (Pujadas et al, 2013) for handling multiscale vessels and improving segmentation speed and accuracy for microvascular analysis (Ward et al, 2013).

ACKNOWLEDGEMENTS

We would like to thank S. Nakagawa and the late Terry Parker in Biomedical Sciences; Lee Buttery and Lisa White in Biomedical Sciences, University of Nottingham, UK for providing the 3D images.

REFERENCES

Bedford, L., Hay, D., Devoy, A., Paine, S., Powe, D. G., Seth, R. & Mayer, R. J. (2008). Depletion of 26S proteasomes in mouse brain neurons causes neurodegeneration and Lewy-like inclusions resembling human pale bodies. *The Journal of Neuroscience*, *28*(33), 8189-8198.

Chanwimaluang, T., & Fan, G. (2003, May). An efficient blood vessel detection algorithm for retinal images using local entropy thresholding. In *Circuits and Systems, 2003. ISCAS'03. Proceedings of the 2003 International Symposium on* (Vol. 5, pp. V-21). IEEE.

Daugman, J. G. (1988). Complete discrete 2-D Gabor transforms by neural networks for image analysis and compression. *Acoustics, Speech and Signal Processing, IEEE Transactions* on, 36(7), 1169-1179.

Ding, Y., Ward, W.O.C., Parker, T., Nakagawa, S., Buttery, L., White, L., Bai, L., (2013). Segmentation of Mouse Brain Microvasculature from Micro-CT Images Using Gabor filter and Local Entropy Thresholding, *International Symposium on Cerebral Blood Flow, Metabolism and Function.*

Frangi, A. F., Niessen, W. J., Vincken, K. L., & Viergever, M. A. (1998). Multiscale vessel enhancement filtering. In *Medical Image Computing and Computer-Assisted Interventation—MICCAI'98* (pp. 130-137). Springer Berlin Heidelberg.

Fraz, M. M., Remagnino, P., Hoppe, A., Uyyanonvara, B., Rudnicka, A. R., Owen, C. G., & Barman, S. A. (2012). Blood vessel segmentation methodologies in retinal images–A survey. *Computer methods and programs in biomedicine.*

Lathen, G., Jonasson, J., & Borga, M. (2008). Phase based level set segmentation of blood vessels. In *19th IEEE International Conference on Pattern Recognition*.

Lim, P. L., Bagci, U., Bai, L. (2013). Introducing Wilmore Flow into Level Set Segmentation of Spinal Vertebrae**,** *IEEE Transactions on Biomedical Engineering***,** Vol. 60, No. 1.

Mallat, S., & Zhong, S. (1992). Characterization of signals from multiscale edges. *IEEE Transactions on pattern analysis and machine intelligence*, 14(7), 710-732.

Osher, S., & Sethian, J. A. (1988). Fronts propagating with curvature-dependent speed: algorithms based on Hamilton-Jacobi formulations. *Journal of computational physics*, *79*(1), 12-49.

Pal, N. R., & Pal, S. K. (1989). Entropic thresholding. *Signal processing*, 16(2), 97-108.

Pająk, R. (2003). Use of two-dimensional matched filters for estimating a length of blood vessels newly created in angiogenesis process. *Opto-Electronics Review*, *11*(3), 237-241.

Pujadas, E. R., & Bai, L. (2013). Non-Euclidean basis function based level set segmentation with statistical shape prior, *IEEE EMBC2013*, Osaka, Japan.

Sato, Y., Nakajima, S., Shiraga, N., Atsumi, H., Yoshida, S., Koller, T., & Kikinis, R. (1998). Three-dimensional multi-scale line filter for segmentation and visualization of curvilinear structures in medical images. *Medical image analysis*, *2*(2), 143-168.

Staal, J., Abràmoff, M. D., Niemeijer, M., Viergever, M. A., & van Ginneken, B. (2004). Ridge-based vessel segmentation in color images of the retina. *Medical Imaging, IEEE Transactions on*, *23*(4), 501-509.

Rorden, C., Karnath, H. O., & Bonilha, L. (2007). Improving lesion-symptom mapping. *Journal of cognitive neuroscience*, *19*(7), 1081-1088.

Ward, W., & Bai, L., (2013). Multifractal Analysis of Microvasculature in Health and Diseases, *IEEE EMBC2013*, Osaka, Japan.